In-process calibration of a non-destructive testing system used for in-process inspection of multi-pass welding

Yashar Javadi[1,2*], Nina E. Sweeney[1], Ehsan Mohseni[1], Charles N. MacLeod[1], David Lines[1], Momchil Vasilev[1], Zhen Qiu[1], Randika K. W. Vithanage[1], Carmelo Mineo[1,3], Theodosia Stratoudaki[1], Stephen G. Pierce[1] and Anthony Gachagan[1]

[1] *Centre for Ultrasonic Engineering (CUE), Department of Electronic & Electrical Engineering (EEE), University of Strathclyde, Glasgow G1 1XQ, UK*

[2] *Department of Design, Manufacturing & Engineering Management (DMEM), University of Strathclyde, Glasgow G1 1XQ, UK*

[3] *Department of Engineering, University of Palermo, Viale delle Scienze, Edificio 8, 90128 Palermo, Italy*

*Corresponding author's email: yashar.javadi@strath.ac.uk

Abstract

In multi-pass welding, there is increasing motivation to move towards in-process defect detection to enable real-time repair; thus avoiding deposition of more layers over a defective weld pass. All defect detection techniques require a consistent and repeatable approach to calibration to ensure that measured defect sizing is accurate. Conventional approaches to calibration employ fixed test blocks with known defect sizes, however, this methodology can lead to incorrect sizing when considering complex geometries, materials with challenging microstructure, and the significant thermal gradients present in materials during the inter-pass inspection period. To circumvent these challenges, the authors present a novel approach to calibration and introduce the concept of in-process calibration applied to ultrasonic Non-Destructive Testing (NDT). The new concept is centred around the manufacturing of a second duplication sample, containing intentionally-embedded tungsten inclusions, with identical process parameters as the main sample. Both samples are then inspected using a high-temperature robotic NDT process to allow direct comparative measurements to be established between the real part and the calibration sample. It is demonstrated that in-process weld defect detection using the in-process calibration technique can more reliably identify defects in samples which would otherwise pass the acceptance test using a traditional calibration.

Keywords: Phased Array Ultrasonic Testing (PAUT); Robotic Welding; Robotic Non-destructive Testing; In-process Calibration; Intentionally Embedded Weld Defects; In-process Welding and Inspection.

1. Introduction

1.1. Non-Destructive Testing (NDT), defect sizing and calibration

To ensure code compliance (e.g., BS EN 1011-1 [1]), weld quality is required to be tested by several quality control methods to ensure there are no defects (lack of fusion, crack, porosity, etc.) above the threshold defined by the acceptance criteria agreed between a manufacturer and client. If the inspection method is carried out non-destructively, known as non-destructive testing (NDT), the component will still be usable in the case that no defect is detected larger than the acceptance criteria. Defect sizing is therefore critical and any NDT report must include the quantitative data to be comparable with the defect size and dimensions specified by the acceptance criteria [2, 3].

Accurate defect sizing is not possible without a controlled and repeatable calibration process in which the signal received from the component defects are compared with a known signal already captured during the inspection of a standard calibration block [4]. This calibration sample requires to be manufactured from as close to identical a material as the component under test and the artificial-defect size and shape must be comparable to the expected defects [5], i.e., a ø1 mm longitudinal lack of fusion in the weld can be represented by a ø1 mm drilled hole in the calibration block.

There are many challenges associated with established calibration methods, these being:

a) Material and defect type: The material can be challenging to realistically duplicate in the calibration block, especially with the growing demands of customised and high-technology components. For example, Javadi et al [6] investigated a dissimilar weld in which four different types of material (i.e., low alloy steel, F22 forging steel, API X65 steel and Inconel) are fused through several welding, buttering and cladding processes. A suitable NDT calibration block for a case like this dissimilar weld is not commonly manufactured. Even if a customised calibration block is manufactured, the next challenge will be a prediction of the defect types expected in each of the four zones and during each of different manufacturing processes [6] to decide about the artificial-defects required to be manufactured in the customised block.
b) Machinability: The artificial-defects in NDT calibration blocks are usually manufactured by machining and drilling processes, leading to the machineability of the target material as another issue of this traditional approach. For example, if the tungsten sample discussed

by Marinelli et al [7] needs to be inspected, it is anticipated that the manufacturing of a calibration block with some small artificial-defects would be impractical due to the hardness of tungsten and its poor machinability [8]. Electro Discharge Machining (EDM) can potentially enhance the machining of hard materials, however, it is still challenging to produce a straight Side-Drilled Hole (SDH) with a small diameter as discussed by Javadi et al [9].

c) Defect geometry: The defect geometry is another practical issue when considering the manufacture of a calibration block. For example, lack of fusion in a real weld is an irregular shaped defect which cannot be perfectly represented by a SDH. Another example is cracking (especially hydrogen cracks) which can have several branches and the crack opening is irregular, yet this crack is often represented by a uniform machined slot in the calibration block [4]. Furthermore, the position of real defects cannot always be reproduced by the machining process. For example, it is impractical to manufacture a blind hole (or slot) to represent an internal crack (or lack of fusion) which is not a surface-breaking feature.

All the above problems of the standard calibration method [1] can be more complex when considering NDT for applications which are not yet standardised, i.e., high-temperature in-process inspection [10, 11] due to the complicated effect which temperature has on the inspection resolution and accuracy [10, 12].

1.2. Phased Array Ultrasonic Testing (PAUT)

Ultrasonic testing is usually implemented using a single element transducer or ultrasonic array, which is a transducer containing more than two individually connected elements. The latter has become increasingly popular during recent years because it can result in higher quality and faster inspection [4]. The advantages of a system using an ultrasonic array, known as Phased Array Ultrasonic Testing (PAUT) system, in comparison with the traditional system using single element transducers are (I) higher inspection flexibility (capability of scanning complex geometry components), (II) faster inspection, (III) synthetic aperture scanning, (IV) synthetic aperture focusing and (V) ability to scan a beam over a range of angles and positions, whilst the transducer remains static [2, 4]. Furthermore, the flexibility of PAUT systems has resulted in advanced developments, such as 3D scanning using two-dimensional arrays [13], complex geometries testing with high-temperature arrays [14] and flexible arrays [15], air-coupled arrays [16, 17], and automated in-process welding and inspection systems [10, 11]. These

developments present potential solutions for difficult scanning scenarios, such as the harsh environments of the nuclear industry [16, 17] and safety critical components in aerospace industries [18].

1.3. Intentionally-embedded tungsten and in-process calibration

Intentionally-embedded tungsten and in-process calibration can offer a solution for a majority of the issues discussed in Sec. 1.1. Embedded-tungsten inclusions can be manufactured in specific, known-sizes and known-shapes which can then be embedded in a predetermined position of the weld length [19] and/or in a specific weld pass. Javadi et al introduced an application of intentionally-embedded tungsten in a weld sample [19] and later in a Wire + Arc Additive Manufacturing (WAAM) component [18]. Using known-size tungsten carbide balls, Javadi et al [18] successfully calibrated a PAUT system to be able to estimate the size and shape of an unknown lack of fusion defect in a WAAM sample. Although the WAAM sample was machined (using drilling) during the manufacturing process [18], Javadi et al [10] introduced another embedding process to place a tungsten rod in the middle of a multi-pass weld without the need for machining of the weld surface. It is then possible to avoid machining of the weld material which is usually difficult to machine due to the high hardness of the weld. Therefore, the intentionally-embedded tungsten process can be considered possible for the majority of weld materials where the material and machinability issues are the main limitation of traditional calibration processes, as discussed in Sec. 1.1.

The in-process calibration focuses on the manufacture of a second duplication sample, a calibration block containing the intentionally-embedded tungsten inclusions, with the same process parameters of the main sample. The calibration sample will then be inspected using a high-temperature in-process inspection to calibrate the NDT system which will be used for accurate, real-time inspection and sizing of the unknown defects in the main sample.

Javadi et al [10] used tungsten rods for the verification of an in-process robotic inspection system. Artificial-defects were embedded in a multi-pass welding process to ensure that the in-process inspection system was sufficiently accurate and capable of detecting common weld defects in real-time. Although the system could successfully detect the tungsten rod in a high-temperature in-process inspection, the sizing procedure of the tungsten inclusion (if it was an unknown-size defect) was not tried and reported [10]. This was due to a combination of problems (e.g., the effect of welding thermal gradient on the ultrasonic wave velocity) which will be discussed in this paper to justify the necessity of the in-process calibration approach.

The experimental works and results of this paper are supported by several manufacturing methods and inspection techniques along with the post-process and simulation algorithms. The high-temperature inspection is implemented using PAUT, in which an ultrasonic array (64 elements) is used rather than a single element probe and, therefore, higher resolution and better imaging performance is expected [4]. Comparative offline inspection is also carried out using the PAUT system alongside Time of Flight Diffraction (TOFD) which provide a 2D map of the defect positions in the weld length [20].

1.4. Alternative methods for the in-process calibration

Scattering matrices were used by Bai et al [3] for ultrasonic characterisation of four test cracks through the use of the correlation coefficient and the structural similarity index as similarity metrics. The accurate characterisation of the crack confirmed that the scale and shift cannot influence the defect characterisation using similarity metrics, therefore, the calibration procedure is not required. Cunningham et al [21] developed a spectral method for sizing cracks using ultrasonic arrays. This method improved the accuracy of crack sizing without the necessity of a numerical model for the scattering matrices. These approaches require further study concerning defect characterisation during in-process inspection and then they could potentially be considered as alternatives for in-process calibration; however, they are not studied in this paper.

2. Experimental setup

2.1. Automated robotic welding

Six specimens were all manufactured from structural steel (S275) plates with dimensions shown in Figure 1a. The specimens were welded using a robotic Tungsten Inert Gas (TIG) welding process with the welding parameters listed in Table 1 and the layout shown in Figure 1b. The robotic welding was equipped by Robot Sensor Interface (RSI) [22] allowing real-time communication between the robot controller and the welding machine. This was critical for achieving Automatic Voltage Correction (AVC) by which the welding voltage can be adjusted with a continuously varied robot Z position (which controls the arc length).

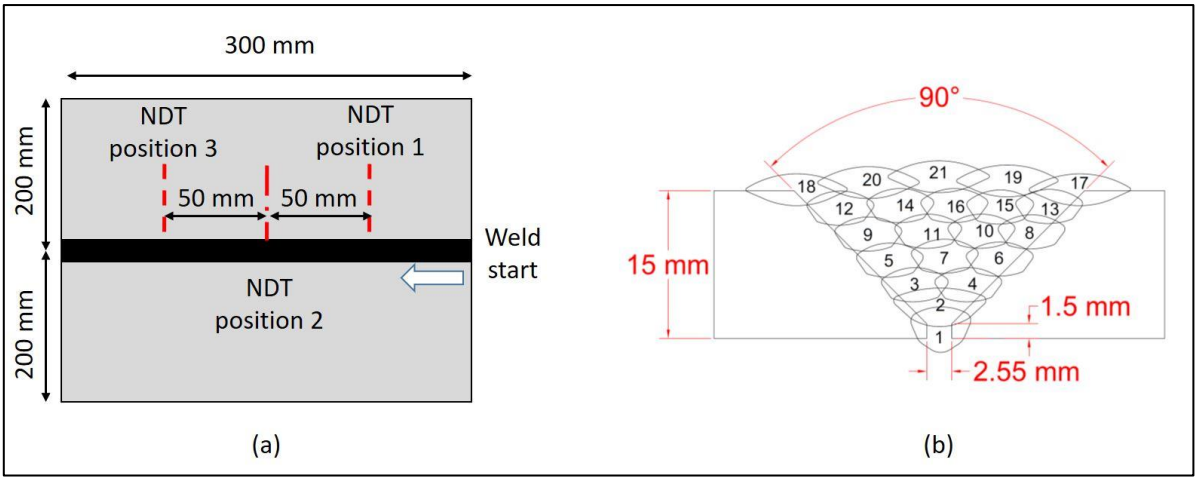

Figure 1. Sample geometry (a) and weld layout (b)

Table 1. Welding parameters

	AVC* set voltage (V)	Current (A)	Travel Speed (mm/min)	Wire Feed Speed (mm/min)	Weaving Amplitude (mm) & Frequency (Hz)
Pass 1	12	120	50	910	2 & 0.3
Pass 2	13.5	220	100	1225	4 & 0.6
Pass 3-16	13.5	210	120	1470	3 & 0.55
Pass 17-21	13.5	240	100	1225	4 & 0.6
** Automatic Voltage Correction (AVC) using the RSI.*					

2.2. In-process inspection and in-process calibration

The six samples were manufactured in pairs, to keep the welding parameters consistency, and tested with intentionally-embedded tungsten defects in each batch. This allowed repeatability testing and also it is in line with the idea of manufacturing an identical sample for in-process calibration. The defects are placed in three predetermined positions in each sample, resulting in six NDT positions as shown in Figure 2a.

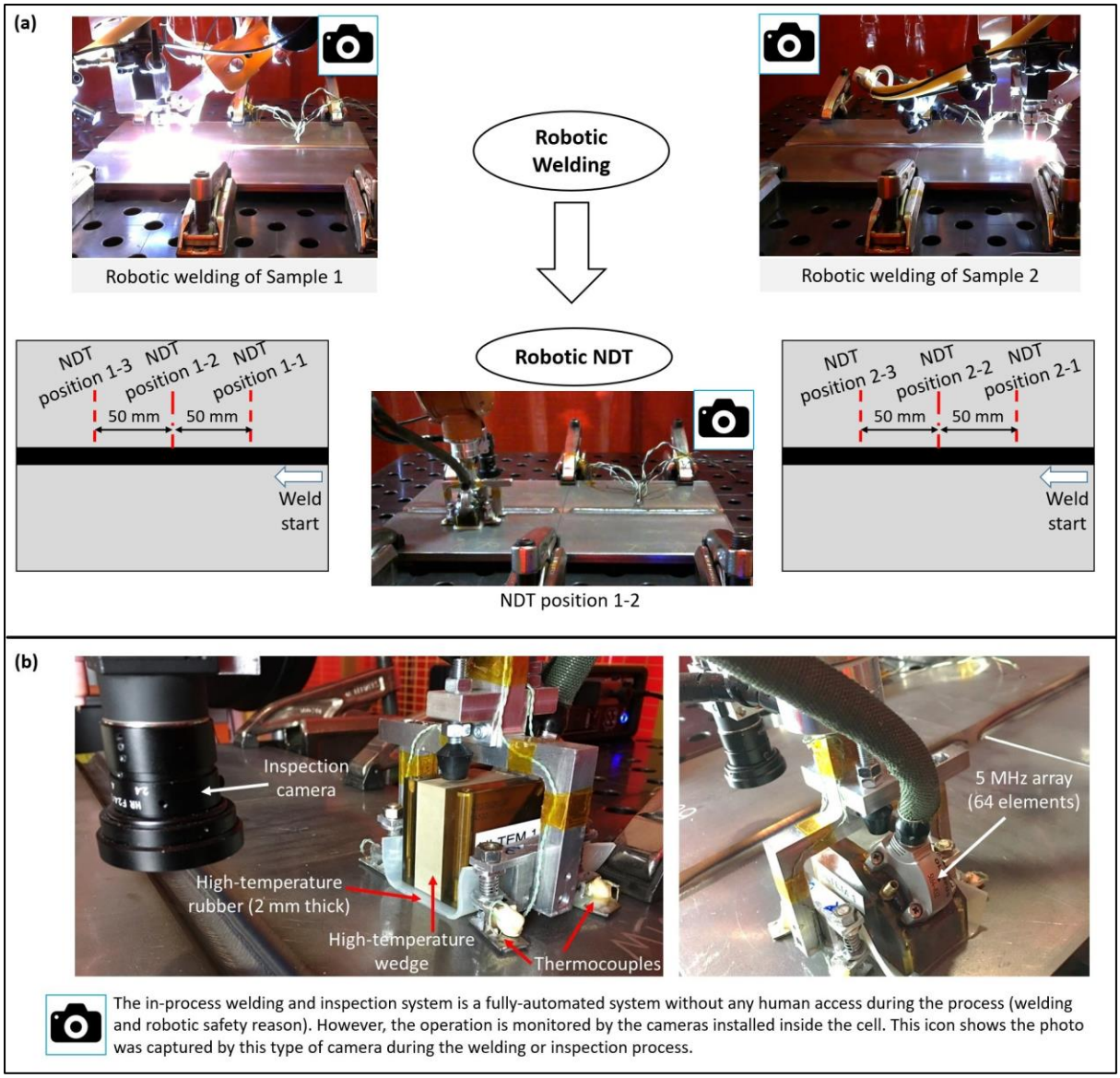

Figure 2. Robotic multi-pass welding and in-process inspection system (a: the whole setup and NDT positions – b: NDT end-effector)

The real-time inspection was carried out after each pass, for a total of 21 welding passes, by a PAUT system which scanned the partially-filled weld in six NDT positions. PAUT sector scanning was implemented using a phased array controller (LTPA by PEAK NDT), a 5 MHz Olympus array (64 elements) mounted on a high-temperature wedge (Olympus ULTEM wedge) and a combination of high-temperature Olympus gel-couplant (between the wedge and rubber) and high-temperature rubber (to avoid potential weld contamination by the liquid couplant) as shown in Figure 2b. Since the inspection end-effector was equipped with high-temperature devices (high-temperature wedge, couplant and rubber), it was possible to carry out the inspection process between the deposition of the welding passes (i.e., when the

specimen surface temperature is 150-180 °C). This allowed for real-time PAUT sector-scanning of the intentionally-embedded defects. The in-process welding and inspection system was the same as that explained by Javadi et al [10], excluding the dry-couplant inspection using rubber which is a recent development introduced by Javadi et al [11].

The setup of in-process calibration is shown in Figure 3. Any calibration process can be started by using a standard calibration block (*Calibration Phase A* as shown in Figure 3). However, as discussed in Section 1.1, many applications need a customised calibration sample, such as the weld with SDH, as shown in *Calibration Phase B* in Figure 3. The problem associated with the welding thermal gradient (discussed in Section 1.1) can reduce the accuracy of using the *Calibration Phase B*, especially for an in-process inspection. Therefore, *Calibration Phase C* (in-process calibration) is studied in this paper. The main difference between *Calibration Phase B* and *Calibration Phase C* is the time of inspection, which is after a destructive SDH machining process in *Calibration Phase B*, while *Calibration Phase C* is a real-time process (no need to stop the manufacturing process to create known size defects destructively).

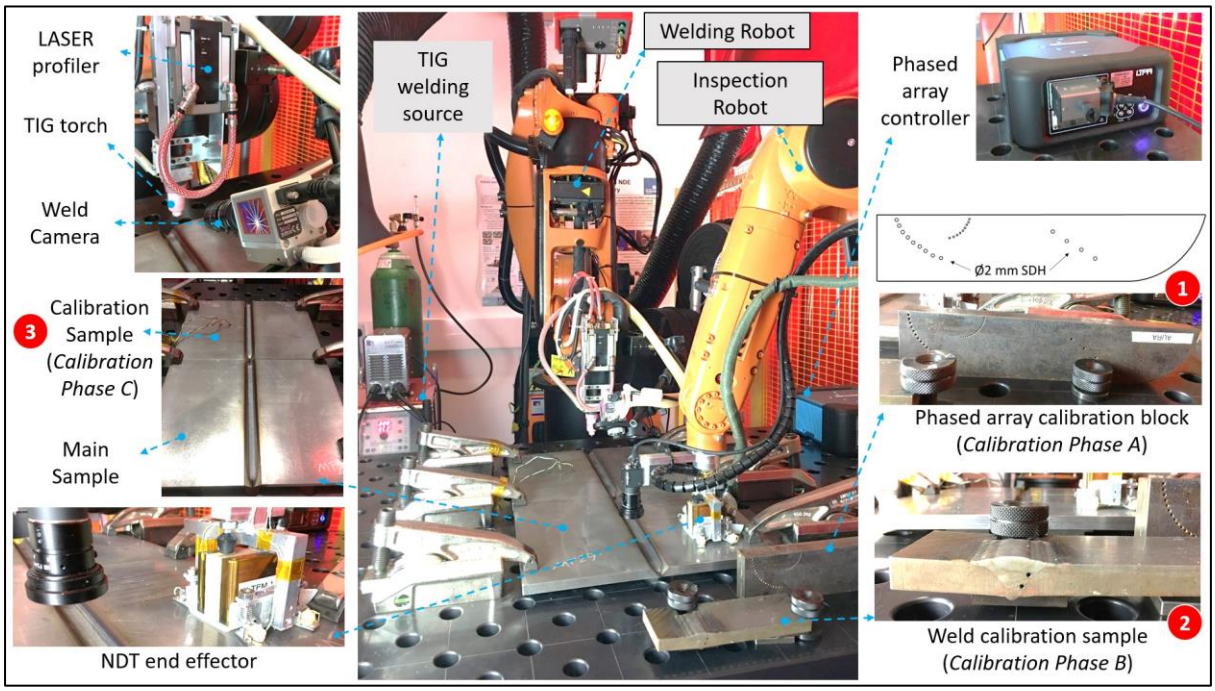

Figure 3. In-process calibration setup

2.3. Intentionally-embedded tungsten process & weld defects

Intentional embedment of tungsten defects was used to produce a range of representative defects in the weld samples. The investigation of various manufacturing methods will ensure the tungsten inclusions can be used as reliable and repeatable calibration artefacts. This

reliability is critical for in-process calibration which relies on the accuracy and repeatability of the defect manufacturing process in the duplicated samples.

Two different methods for introducing the tungsten defects were considered, these were using a drilling technique for considering vertically aligned defects, and angle grinding to represent horizontally aligned defects (lack of fusion, inclusions and cracks) in the weld region (see Table 2).

Table 2. Represented weld defect and intentionally-embedded tungsten procedure

Defect code	Represented weld defect	Intentionally-embedded tungsten procedure
D1	Vertical blind hole (representing a vertical crack)	1) Drilling a ø3 mm hole (depth: 9.5 mm) 2) Using a ø3 mm tungsten ball on top of the hole to block the melt filling it
G1	Controllable-size and controllable-shape lack of fusion	1) Machining a slot (deepest section: 5.3 mm depth) 2) Using a ø2.4 mm tungsten rod on top of the slot to avoid the melt flowing inside the slot
G2	Inclusion	1) No machining or grinding 2) Dividing the 280 mm weld length to two 125 mm length welds to leave 30 mm blank space in the weld length centre 3) Putting a 30 mm length tungsten rod (ø2.4 mm) surrounded by some amount of iron powder
G3	Crack	1) Grinding two oriented narrow slot using a 1 mm thick Dremel cutting disk 2) Using a ø1 mm tungsten rod on top of each slot to avoid the melt flowing inside the slot
G4	Oriented lack of fusion (controllable size and shape)	1) No machining or grinding 2) Dividing the 280 mm weld length to two 125 mm length welds to leave 30 mm blank space in the weld length centre 3) Putting a 30 mm length tungsten pipe (OD: ø3 mm; ID: ø2 mm) in an oriented way (30-degree in comparison with the weld line)
G5	Sidewall lack of fusion (controllable size and shape)	1) Machining a slot (deepest section: 3 mm depth) in the side of the weld 2) Putting a 30 mm length tungsten pipe (OD: ø3 mm; ID: ø2 mm) surrounded by some amount of iron powder

The position and manufacturing procedure implemented during the embedding of D1 is shown in Figure 4. The welding camera images proved that the hole was properly blocked by the tungsten ball and the melt was unlikely to penetrate into the hole. These images also show the

stability (its shape and position) of the tungsten carbide ball against the high-temperature arc passing adjacent to the ball.

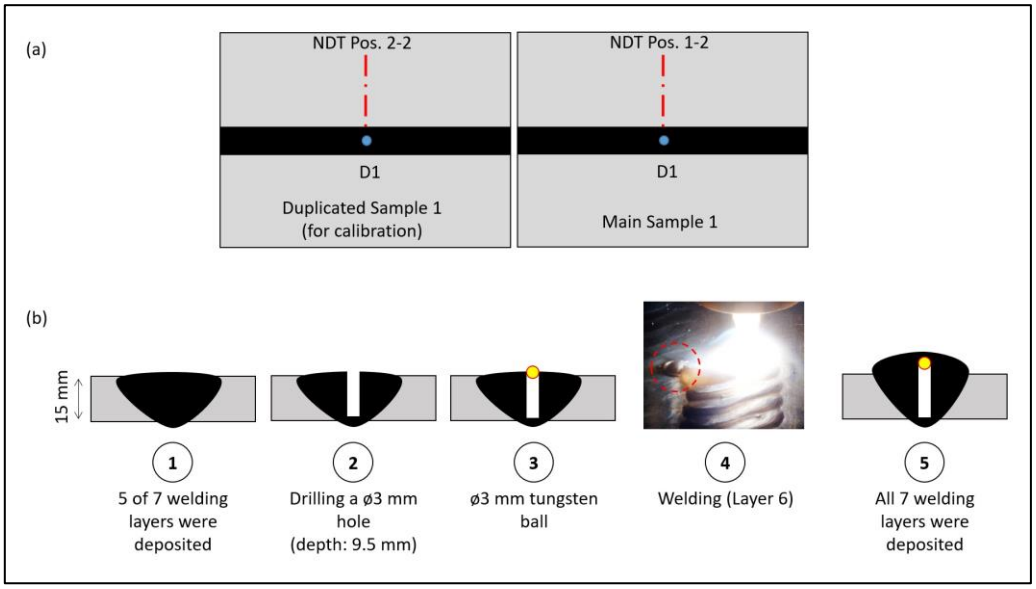

Figure 4. Position (a) and procedure (b) of the intentionally-embedded tungsten ball (D1)

Using an angle grinder, the intentional embedding process of a lack of fusion, crack and inclusion were introduced (see Figure 5). If the intentionally-embedded tungsten inclusions are to be used for calibration purposes, they are expected to repeatably reflect a consistent ultrasonic amplitude. For example, if a ø2 mm tungsten rod were going to be used for the calibration, the procedure would include measurement of a ø2 mm SDH in a standard calibration block and a comparison with the signal received from the tungsten rod in the weld. The ratio between these two signals would then be used to size an unknown defect. However, this process would assume that the tungsten rod was a known-size defect which could be embedded in the weld with a repeatable process. Therefore, if the tungsten were not fused completely to the weld, with some unknown amount of air-gap left around it, the calibration process would be compromised [18]. It is then critical to ensure there is a minimum amount of air-gap around the tungsten to realistically achieve zero air-gap after the weld deposition. Iron powder was used in this work for filling small gaps (see G2 and G5 in Figure 5). However, large gaps must be avoided as the iron powder cannot effectively fill them. This will be discussed more in the results section.

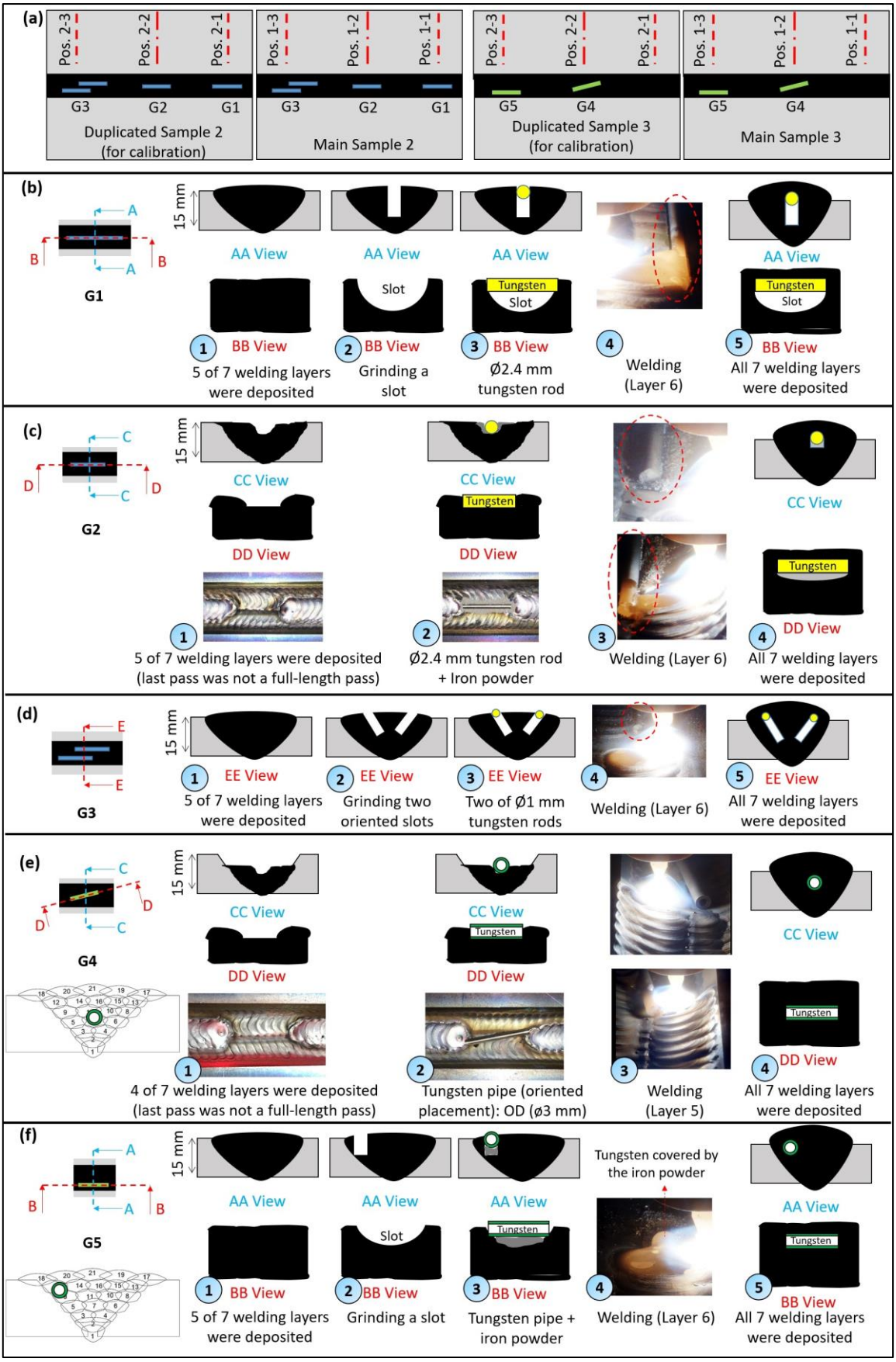

Figure 5. Position (a) and procedure (b-f) of the intentionally-embedded defects (G1-G5)

Once the air-gaps around the tungsten are fully eliminated, the reflection amplitude of the tungsten material will play a critical role in the inspection of the intentionally-embedded defects. As discussed by Javadi et al [18], an ultrasonic gain of 53 dB was required to detect a ø3 mm tungsten ball while only 41 dB was enough for the detection of a smaller size SDH (ø1.5 mm). This shows that the reflection amplitude from tungsten, in comparison with air, is weaker, as expected. This will be more challenging once the tungsten is used for in-process inspection where the high-temperature can negatively influence the signal amplitude. Therefore, it is recommended to use tungsten pipes rather than tungsten rods (see Figure 5e, f). In this example, a tungsten pipe with ø2 mm internal diameter is envisaged to be equivalent to a ø2 mm SDH, albeit a small amount of energy will be reflected from the tungsten wall itself (pipe wall thickness is 1 mm). However, the key benefit of an intentionally-embedded tungsten pipe against a post-manufacture SDH, is the possibility of having a blind hole inside the weld with a controllable orientation angle, as shown in Figure 5e.

3. Results and discussions

3.1. Intentionally-embedded tungsten process & weld defects

The PAUT sector scanning, TOFD and macrographs of the intentionally-embedded tungsten methods evaluated in this work are shown in Figure 6. The controllable-size defects successfully produced and detected (using PAUT and TOFD) in the predetermined positions, show that the intentionally-embedded tungsten method can potentially be used as an accurate calibration procedure. The methods shown in Figure 6 have all demonstrated that there are various methods to embed an intentional defect in the weld ensuring that they can be successfully detected using the ultrasonic NDT method. This was underpinned by the high reflection amplitude in the PAUT sector scans which show that, even if the tungsten itself is not a perfect ultrasonic reflector (see G2 in Figure 6), there are some practical methods to produce air-filled defects of controllable size (see D1, G1 and G3-5 in Figure 6). All of these defects were successfully detected using the high-temperature in-process inspection system, however, it is not possible to show all results in this paper (inspection of six samples, in six NDT positions, after each of 21 weld passes has produced 756 weld images).

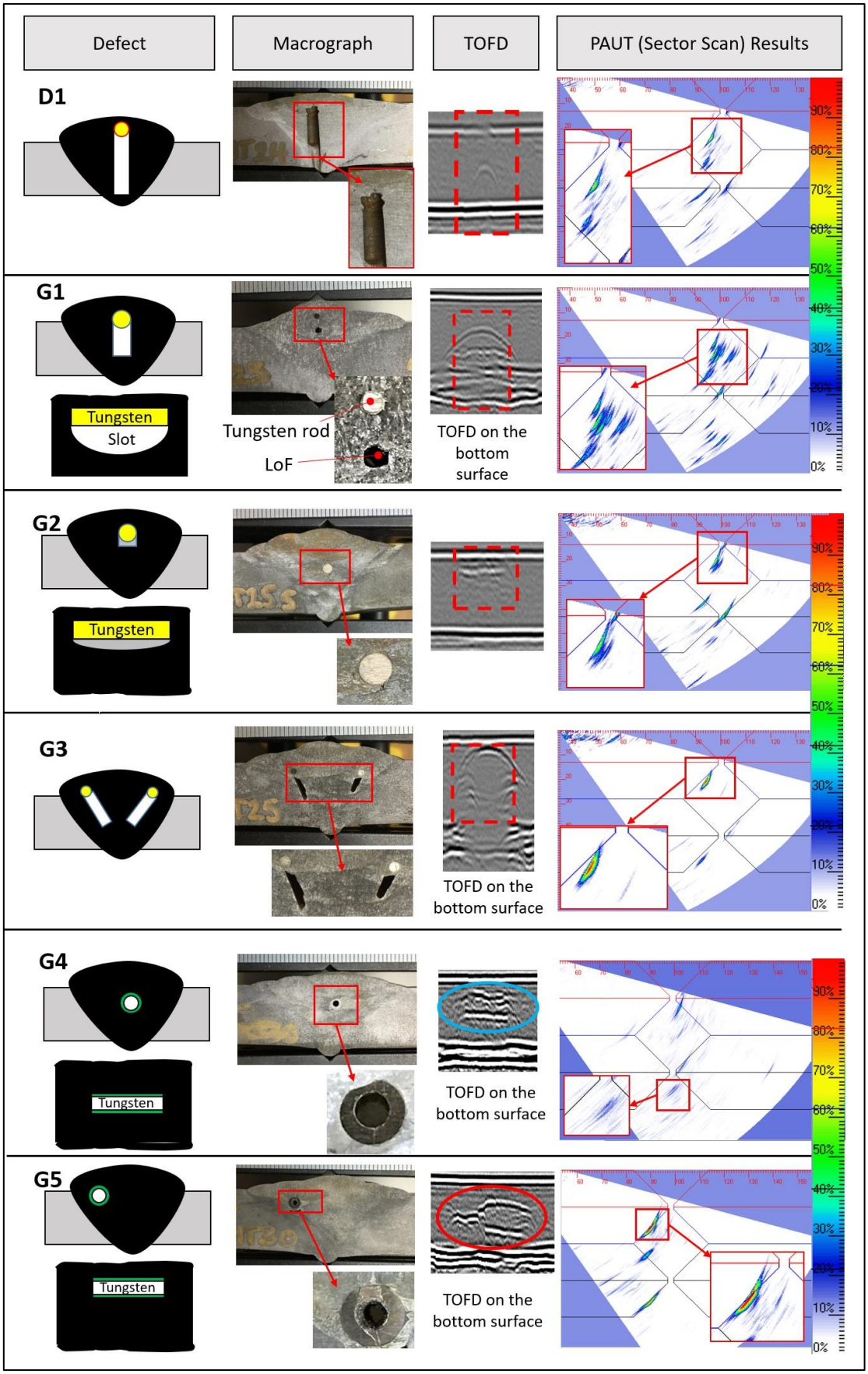

Figure 6. Investigation of various intentionally-embedded tungsten methods for simulation of weld defects

The above methods are presented as some examples of the intentionally-embedded tungsten process. Importantly, this is a flexible process and many more concepts can be incorporated, especially when the tungsten is used as both a lid (to block the melt) and an inclusion. However, it is noted that the majority of the artificial defects explored in this paper are categorised as volume-type defects and that area-type defects also require consideration and, as such, will require further study in the future. The minimum defect size detected in this work was a slot produced by ø1 mm tungsten rod (G3); however, previous work using the same PAUT system highlighted its ability to detect smaller defects [10] and even tiny hydrogen cracks [11]. Although, the possibility of manufacturing small defects and cracks in a repeatable way suitable for in-process calibration requires further investigation.

As shown in Figure 6 (G4 and G5), the tungsten pipe was successfully detected with all the inspection methods (PAUT sector scanning, TOFD, and in-process inspection) while a comparison between G2 and G5 proves that the signal from the tungsten pipe is expectably stronger than that of the tungsten rod. The macrographs showed that the pipes internal region had not been filled with any material and therefore a blind horizontal hole had been successfully embedded inside the weld using this method. The microscopic investigations (Figure 7a) showed that the tungsten pipe wall was slightly deformed due to the welding temperature. However, the key purpose was to embed a blind hole, of known diameter inside the weld and, hence, this small deformation can be ignored as it does not affect the internal diameter. The application of tungsten pipe and iron powder was proved to be practical through microscopic investigation (see Figure 7b) since all three materials (weld, iron powder and tungsten) are completely fused.

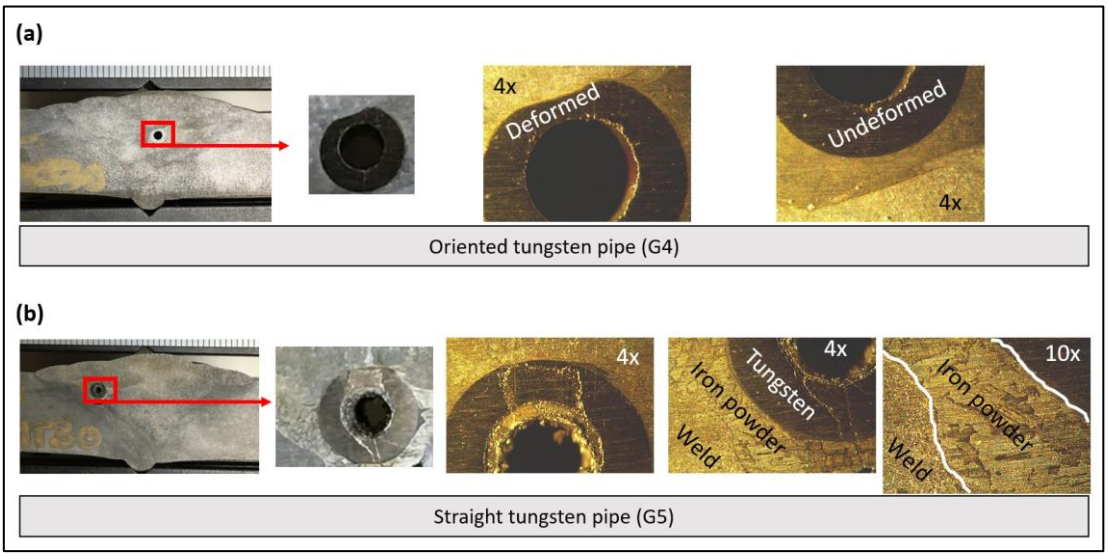

Figure 7. Microscopic investigation of the intentionally-embedded tungsten pipes (a: defect code G4 and b: defect code G5)

Application of iron powder is recommended to avoid air-filled gaps around the tungsten. However, this technique must be used carefully, as air gaps are not apparent at the macroscopic level, however, some air defects are visible at a microscopic level (see Figure 8a). This method is still significantly better than welding without iron powder (see Figure 8b). It is always preferable to allow the melt to flow smoothly around the tungsten surface however, this occurs more readily around a light-weight and small-size tungsten inclusion (see Figure 8c) and for the large-size tungsten, the iron powder addition is used in this work as the best current solution.

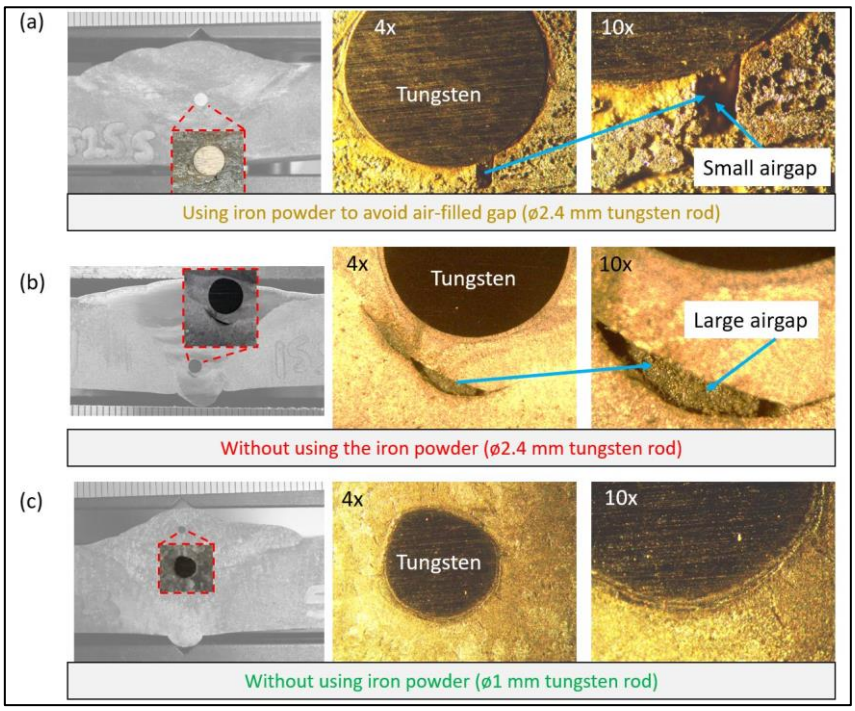

Figure 8. Using the iron powder to avoid the air-filled gap around the tungsten rod

3.2. In-process calibration

3.2.1. Justification and necessity of in-process calibration

Javadi et al [10] have shown that the ultrasonic inspection results can be considerably influenced by temperature. For example, the defect position (an intentionally embedded tungsten pipe) was 3 mm different between two inspections carried out at 28° C and 164° C. They also reported a considerable change in the reflection amplitude, from 62% to 25%, with this temperature range. Subsequently, if the calibration is traditionally performed at room temperature, which is the most common current method in industry, the results cannot be used directly for a high-temperature inspection. Hence, it is clear that as the in-process inspection is

performed at a high temperature (150-180° C in this work), then a high-temperature calibration process is required.

It can be argued that the temperature effect on the ultrasonic wave properties (and hence defect detection/imaging) is a well-known parameter [23], which can be measured [10] and then compensated for during in-process inspection. However, this is challenging in real-world applications where the thermal gradient is not well characterised, such as in complex geometry components. To illustrate this problem, four thermocouples (type K) were installed on the opposite side of the weld and positioned within an area matching the ultrasonic array footprint (see Figure 9a). The temperature profile recorded by these thermocouples is shown in Figure 9b. These show that the ultrasonic beam paths from the angle beam transducer were travelling through a varying temperature distribution, which was also continuously changing in time. Even if the temperature effect can be compensated for in a traditional calibration process, it will still be very difficult to repeat the main inspection at the exactly same time and temperature to take full benefit of the calibration. Therefore, the in-process calibration method, in which the timing and temperature gradient are the same in the main and duplicated sample, can be considered as a solution for the complicated thermal gradient problem.

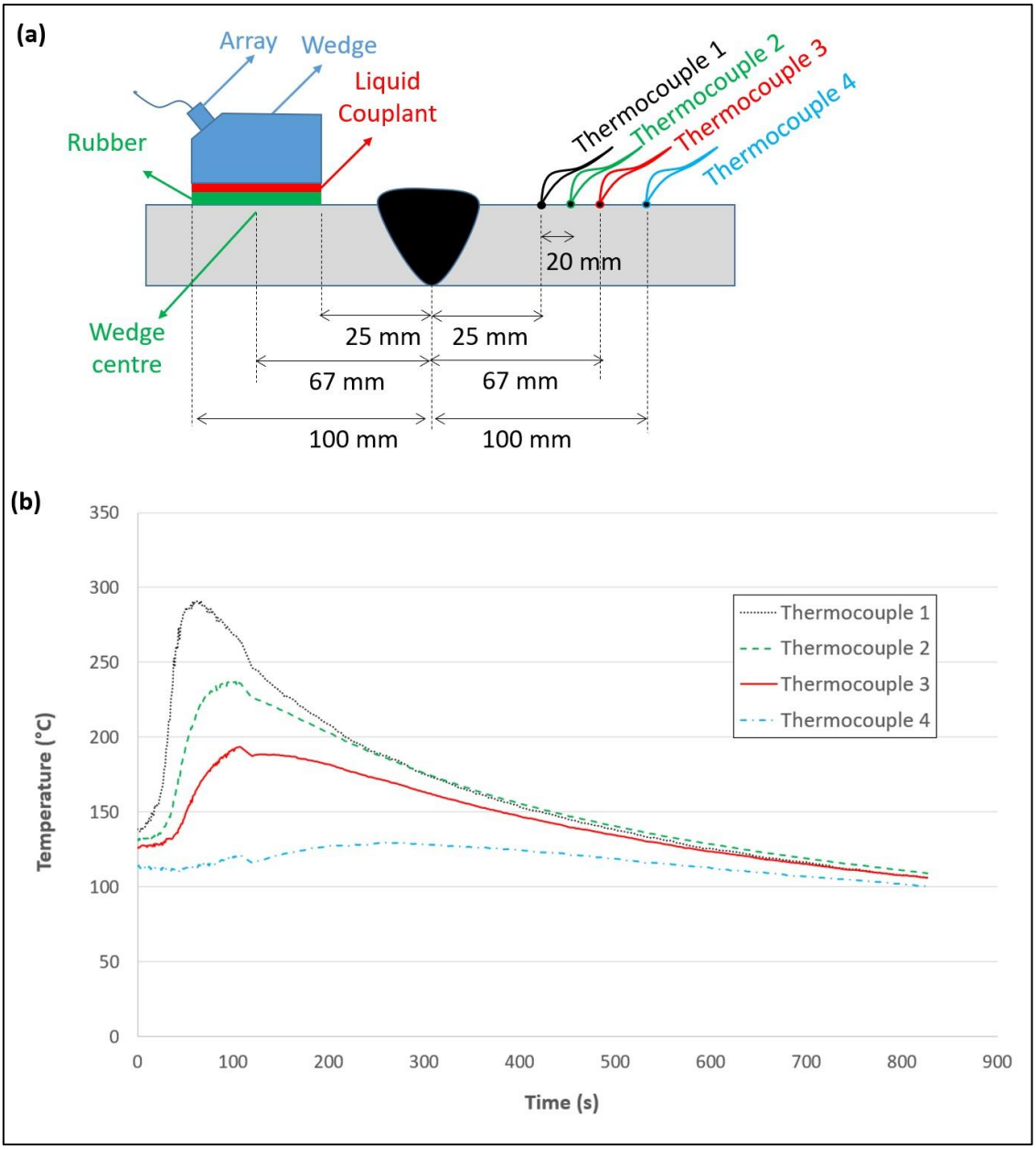

Figure 9. Time dependence of the thermal distribution of the welding process (a: thermocouples position – b: thermocouples measurement results)

3.2.2. Comparing in-process calibration against traditional calibration

It was first assumed that a traditional calibration method would be used for the high-temperature in-process inspection investigated in this study. The PAUT system was initially calibrated against the weld calibration sample (*Calibration Phase B* in Figure 3). The calibration results are shown in Figure 10. The authors employed good practice to normalise the sector scanning images to 80% of the maximum reflection amplitude [18], thus avoiding

any potential saturated gain problem in subsequent scans of the main sample. The results showed that a gain of 54 dB and 57 dB were required for the detection of ø2 mm SDHs machined in different places of the weld (see Figure 10). The inspection was then required to be compared with these results, i.e., any defect detected with a gain <54 dB in a position close to the root could be sized as a >ø2 mm defect. This procedure was followed for the high-temperature inspection of a sample with the oriented tungsten and partially-filled weld until pass 9 (see Figure 11). For the sizing of the defect (G4 in Figure 11), the reflection amplitude was compared with the reference defect (a comparable defect like a ø2 mm SDH in the calibration sample) and if there was a defect passing the threshold (54 dB in this case), it could be sized larger than ø2 mm. If it had been assumed that the acceptance criteria is a ø2 mm defect size, the sample with G4 was acceptable because the signal received from the defect was much weaker than the reference signal expected from a ø2 mm defect (see Step 1-5 in Figure 11). However, as shown in Figure 5e, it was known that a tungsten pipe had been embedded inside the sample and then at least a ø2 mm defect size should have been detected. Therefore, it can be concluded that the traditional calibration approach was unsuccessful to detect a ø2 mm defect during an in-process high-temperature inspection.

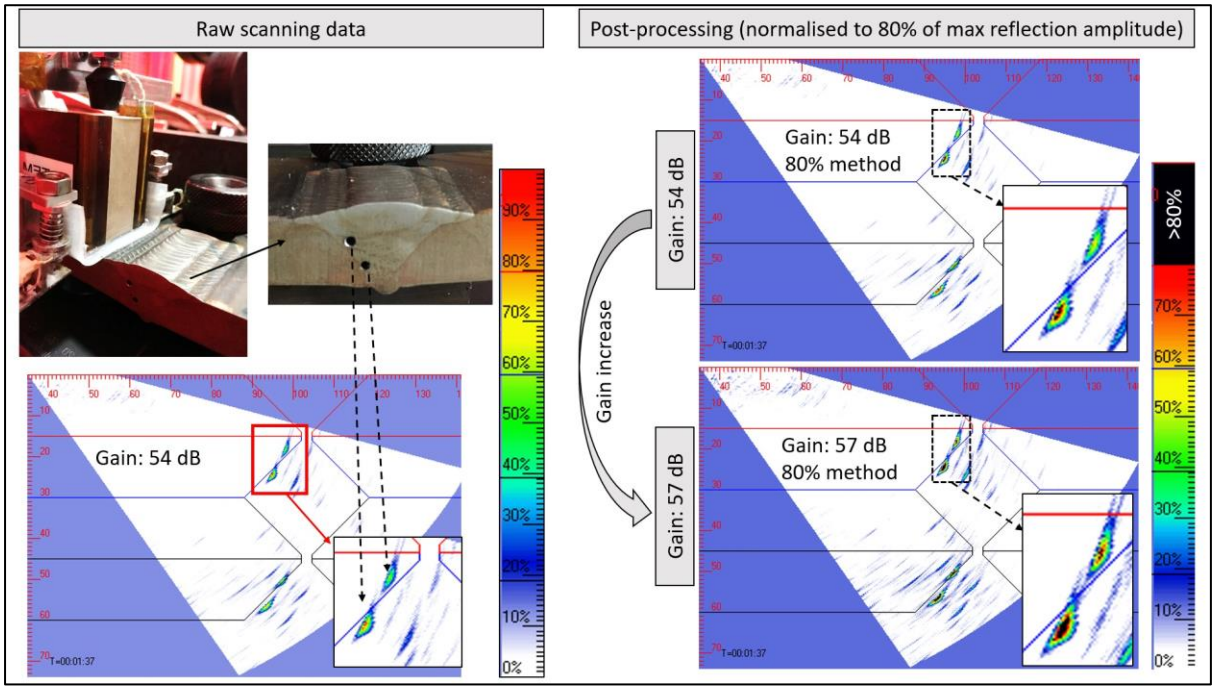

Figure 10. Results of the *Calibration Phase B*

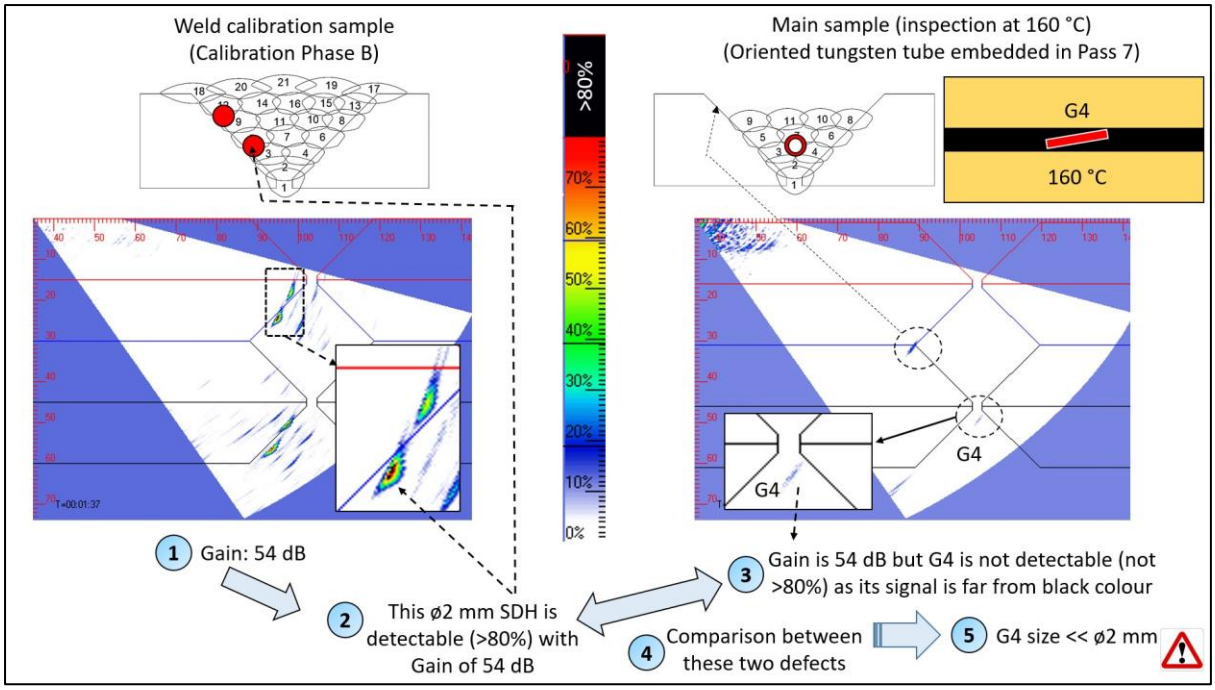

Figure 11. High-temperature in-process inspection using the traditional calibration approach

The sample, which was incorrectly accepted with the use of traditional calibration, will be rejected if an in-process calibration is used, see Figure 12. This shows that if an identical sample with the same expected defects is manufactured simultaneously, a real-time gain adjustment (74 dB shown in Figure 12) can ensure that the defect is not misinterpreted using the high-temperature in-process inspection system. The procedure will then include: (I) embedding an intentional defect in the duplicated calibration sample, representing the defect size and type specified in the acceptance criteria, (II) adjust the gain, in each pass based on the inspection temperature, to detect the intentional defect and (III) use the real-time adjusted gain for the inspection of the main sample.

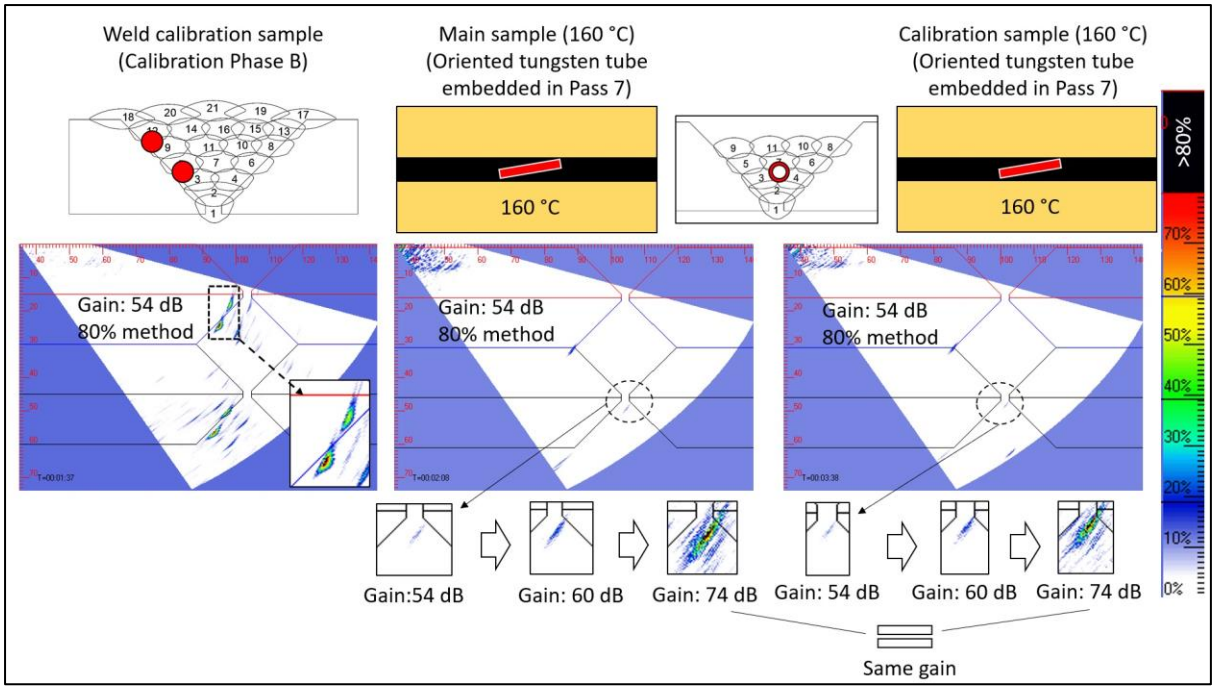

Figure 12. In-process calibration results (sample with the oriented tungsten pipe)

It can be argued that a straight SDH in the weld calibration is compared with an oriented tungsten pipe and these incomparable features are not enough to prove that *Calibration Phase B* is not a suitable approach. It is worth mentioning that *Calibration Phase B* is a standard method largely used in industry [2] and SDH are usually manufactured in a straight way since it is hard to predict the orientation of practical unknown defects in components. This highlights one of the advantages of in-process calibration by which the defect orientation can also be investigated. Furthermore, the same comparison of *Calibration Phase B* and in-process calibration for the straight tungsten is shown in Figure 13. This again shows that setting the in-process inspection gain on 54 dB (traditional calibration method) could simply result in misinterpretation of this defect size, while it was learnt from the in-process calibration that the correct gain must be 62 dB.

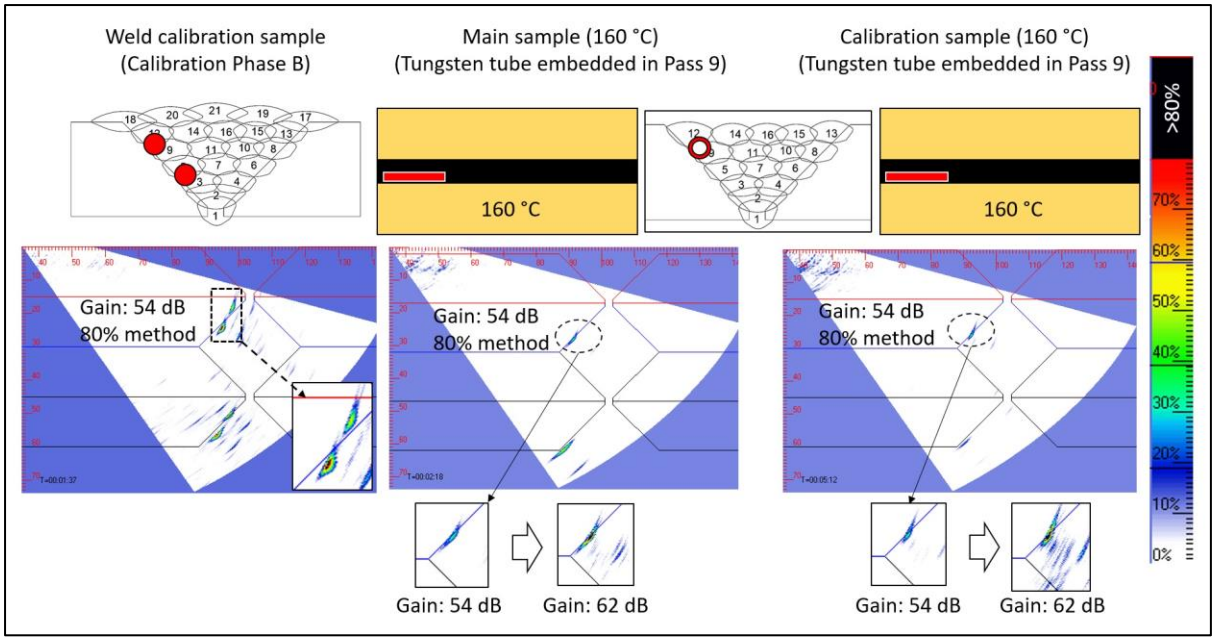

Figure 13. In-process calibration results (sample with the straight embedded-tungsten)

4. Conclusions

In this paper, a combination of: in-process inspection, intentionally-embedded tungsten defects, PAUT inspection, TOFD and multi-pass robotic welding is employed to study the feasibility of using an in-process calibration method. Based on the results, it can be concluded that:

1) The intentionally-embedded tungsten process was used successfully to embed several features which are challenging to manufacture with any other method. For example, controllable-size vertical and horizontal blind holes, and oriented blind slot were all successfully manufactured and inspected with a range of methods and approaches (PAUT, TOFD, metallography and microscopic investigations).
2) Two main improvements were introduced to facilitate the use of intentionally-embedded tungsten for in-process calibration. These included: (I) using iron powder to avoid forming air-filled gaps around the tungsten and (II) tungsten pipe was used to enhance the ultrasonic reflection amplitude. The latter was based on a comparison between the weak signal received from the tungsten material with a very strong signal from the air-filled features (e.g., tungsten pipe with an internal diameter of ø2 mm). The tungsten pipe was not filled with the weld material during the welding and

remained in the form of a pipe, regardless of its thin wall, after the welding. These were critical to accept it as a good ultrasonic reflector.

3) Using the high-temperature in-process inspection system, the in-process calibration and traditional calibration methods were compared to detect a tungsten pipe (ø2 mm internal diameter) intentionally embedded in the weld. It was found that the sample could be incorrectly accepted with the traditional calibration approach while the tungsten pipe was detected, and the sample was rejected, using the in-process calibration.

It is worth mentioning that in-process calibration can be used for in-process inspection using any NDT system (not only ultrasonic which was considered in this paper). The idea was justified in this paper with several case studies and a combination of robotic welding and inspection system. However, the process needs to be enhanced through further investigations into the manufacture of smaller and area-type defects, alongside an automated defect embedding process. Future consideration should also be given to the extension of this in-process calibration technique into other NDT applications, components and manufacturing processes.

5. Acknowledgement

This work was undertaken as part of the UK Research Centre in NDE (RCNDE – EP/L022125/1) core project (ABC of ARC) and also RCNDE3 core research Feasibility Project (entitled “Test Samples to Support Developments in High-Temperature In-Process Inspection”). Furthermore, the concept of high-temperature in-process inspection will be used in the Wire + Arc Additive Manufacturing (WAAM) projects which are all supported by EPSRC and InnovateUK as follows: (I) NEWAM (EP/R027218/1), (II) AIMaReM (EP/N018427/1) and (III) RoboWAAM (EP/P030165/1). The authors then like to acknowledge EPSRC, InnovateUK and RCNDE for the support and funding of the projects.

6. Data availability

The data that support the findings of this study are available from the corresponding author on reasonable request.

7. References

[1] B. STANDARD, Welding - Recommendations for welding of metallic materials, Part 2: Arc welding of ferritic steels, BSI Group, UK, 2009.
[2] P. Cawley, Non-destructive testing - current capabilities and future directions, Proc. Inst. Mech. Eng. Pt. L-J. Mater.-Design Appl. 215 (2001) 213-223.
[3] L. Bai, A. Velichko, B.W. Drinkwater, Ultrasonic Characterization of Crack-Like Defects Using Scattering Matrix Similarity Metrics, Ieee Transactions on Ultrasonics Ferroelectrics and Frequency Control 62 (2015) 545-559.
[4] B.W. Drinkwater, P.D. Wilcox, Ultrasonic arrays for non-destructive evaluation: A review, Ndt & E International 39 (2006) 525-541.
[5] P.J. Shull, Nondestructive evaluation: theory, techniques, and applications, CRC press2002.
[6] Y. Javadi, J.N. Walsh, A. Elrefaey, M.J. Roy, J.A. Francis, Measurement of residual stresses induced by sequential weld buttering and cladding operations involving a 2.25Cr-1Mo substrate material, International Journal of Pressure Vessels and Piping 154 (2017) 58-74.
[7] G. Marinelli, F. Martina, H. Lewtas, D. Hancock, S. Ganguly, S. Williams, Functionally graded structures of refractory metals by wire arc additive manufacturing, Science and Technology of Welding and Joining 24 (2019) 495-503.
[8] M. Ottersbach, W. Zhao, Experimental Investigations on the Machinability of Tungsten Carbides in Orthogonal Cutting with Diamond-coated Tools, Procedia CIRP 46 (2016) 416-419.
[9] Y. Javadi, C.N. MacLeod, S.G. Pierce, A. Gachagan, W. Kerr, J. Ding, S. Williams, M. Vasilev, R. Su, C. Mineo, J. Dziewierz, Ultrasonic phased array inspection of wire plus arc additive manufacture (WAAM) samples using conventional and total focusing method (TFM) imaging approaches, Insight 61 (2019) 144-148.
[10] Y. Javadi, E. Mohseni, C.N. MacLeod, D. Lines, M. Vasilev, C. Mineo, E. Foster, S.G. Pierce, A. Gachagan, Continuous monitoring of an intentionally-manufactured crack using an automated welding and in-process inspection system, Materials & Design 191 (2020) 108655.
[11] Y. Javadi, N.E. Sweeney, E. Mohseni, C.N. MacLeod, D. Lines, M. Vasilev, Z. Qiu, C. Mineo, S.G. Pierce, A. Gachagan, Investigating the effect of residual stress on hydrogen cracking in multi-pass robotic welding through process compatible non-destructive testing, Journal of Manufacturing Processes (2020).
[12] A. Chabot, N. Laroche, E. Carcreff, M. Rauch, J.-Y. Hascoët, Towards defect monitoring for metallic additive manufacturing components using phased array ultrasonic testing, Journal of Intelligent Manufacturing (2019).
[13] Y. Mendelsohn, E. Wiener-Avnear, Simulations of circular 2D phase-array ultrasonic imaging transducers, Ultrasonics 39 (2002) 657-666.
[14] K.J. Kirk, A. McNab, A. Cochran, I. Hall, G. Hayward, Ultrasonic arrays for monitoring cracks in an industrial plant at high temperatures, Ieee Transactions on Ultrasonics Ferroelectrics and Frequency Control 46 (1999) 311-319.
[15] S. Chatillon, G. Cattiaux, M. Serre, O. Roy, Ultrasonic non-destructive testing of pieces of complex geometry with a flexible phased array transducer, Ultrasonics 38 (2000) 131-134.
[16] A. Neild, D.A. Hutchins, T.J. Robertson, L.A.J. Davis, D.R. Billson, The radiated fields of focussing air-coupled ultrasonic phased arrays, Ultrasonics 43 (2005) 183-195.
[17] A. Gachagan, S. Kelly, M. Altman, E. Grauvogl, G. Hayward, R. Banks, T. McCunnie, D. Skillen, Development of a manual air-coupled ultrasonic inspection instrument for use on aeronautical structures under in-service conditions, Review of Progress in Quantitative Nondestructive Evaluation, Vols 22a and 22b 20 (2003) 883-890.
[18] Y. Javadi, C.N. MacLeod, S.G. Pierce, A. Gachagan, D. Lines, C. Mineo, J. Ding, S. Williams, M. Vasilev, E. Mohseni, R. Su, Ultrasonic phased array inspection of a Wire + Arc

Additive Manufactured (WAAM) sample with intentionally embedded defects, Additive Manufacturing 29 (2019) 100806.
[19] Y. Javadi, M. Vasilev, C.N. MacLeod, S.G. Pierce, R. Su, C. Mineo, J. Dziewierz, A. Gachagan, Intentional weld defect process: From manufacturing by robotic welding machine to inspection using TFM phased array, AIP Conference Proceedings 2102 (2019) 040011.
[20] F.W.T. Yeh, T. Lukomski, J. Haag, T. Clarke, T. Stepinski, T.R. Strohaecker, An alternative Ultrasonic Time-of-Flight Diffraction (TOFD) method, Ndt & E International 100 (2018) 74-83.
[21] L.J. Cunningham, A.J. Mulholland, K.M.M. Tant, A. Gachagan, G. Harvey, C. Bird, A spectral method for sizing cracks using ultrasonic arrays, Inverse Problems in Science and Engineering 25 (2017) 1788-1806.
[22] KUKA, KUKA RobotSensorInterface (RSI) 3.2 Documentation , in: KUKA (Ed.) Version: KST RSI 3.2 V1, 2013.
[23] F.A. Silber, C. Ganglbauer, ULTRASONIC TESTING OF HOT WELDS, Non-Destructive Testing 3 (1970) 429-+.